Available online at www.sciencedirect.com
SCIENCE DIRECT®
Journal of Solid State Chemistry 177 (2004) 2803–2809
JOURNAL OF SOLID STATE CHEMISTRY
http://elsevier.com/locate/jssc

On the mechanism of the P2−$Na_{0.70}CoO_2$→O2−$LiCoO_2$ exchange reaction—Part II: an in situ X-ray diffraction study

F. Tournadre,[a] L. Croguennec,[a,*] P. Willmann,[b] and C. Delmas[a]

[a] *Institut de Chimie de la Matière Condensée de Bordeaux-CNRS and Ecole Nationale Supérieure de Chimie et Physique de Bordeaux, Université Bordeaux I, 87 Av. du Dr A. Schweitzer, 33608 Pessac Cedex, France*
[b] *Centre National d'Etudes Spatiales, 18 Av. Edouard Belin, 31401 Toulouse Cedex 4, France*

Received 13 October 2003; received in revised form 13 April 2004; accepted 18 April 2004

Abstract

A model was proposed to describe the exchange reaction of sodium by lithium in P2 crystals, it was based first on the formation of nucleation centers and then on the growth of O2 domains in P2 crystals from these nucleation centers. This study has shown that depending on the ratio between the growing and nucleation speeds, O2, O6 or faulted structures are obtained and that this model allows a good analysis of the exchange process. XRD patterns simulation and their comparison with that of experimental O2–$LiCoO_2$ have shown that there was almost no defects in the O2–$LiCoO_2$ structure obtained by ion exchange in water. Therefore, this study has shown that the growth of the O2 domains in the P2−$Na_{0.7}CoO_2$ crystals is faster than the formation of nucleation centers.

This P2−$Na_{0.7}CoO_2$→O2−$LiCoO_2$ exchange reaction was also studied in situ by X-ray diffraction; simulations of key XRD patterns by P2−O2 intergrowths were also achieved. It was shown, in good agreement with the simulations, that the growth of O2 domains was faster than the formation of the nucleation centers and kinetically activated by a P2−$Na_{0.70}CoO_2$→P2*−$Na_{\sim 0.50}CoO_2$ phase transition. For those reasons, the P2−$Na_{0.70}CoO_2$→O2−$LiCoO_2$ exchange reaction in water leads to an O2 phase, with an almost ideal packing.

Keywords: Layered oxides; $LiCoO_2$; Ion exchange reaction; Electrode material; Stacking faults; In situ X-ray diffraction

1. Introduction

The ion exchange reaction in the Na_xMO_2 phases is an alternative way to synthesize new lamellar lithiated phases. O2−$LiCoO_2$ was the first metastable phase obtained by ion exchange from sodium to lithium reaction in P2−$Na_{0.70}CoO_2$ [1]. In addition to $LiCoO_2$, T#2−$Li_{2/3}[Ni_{1/3}Mn_{2/3}]O_2$ [2] and recently found T#2−$Li_{2/3}[Co_{2/3}Mn_{1/3}]O_2$ [3] are well crystallized. All other phases: O2−$LiMnO_2$ [4], $Li_{0.70}[Mg_{0.30}Mn_{0.70}]O_2$ [5] and those belonging to the $Li_{2/3}[Ni_{1/3-x}Co_xMn_{2/3}]O_2$ and $Li_{2/3}[Ni_{1/3-x/2}Co_xMn_{2/3-x/2}]O_2$ families exhibit more or less stacking faulted structures [6]. Chowdari et al. were also interested in O2-type structures and studied the influence on the electrochemical performances of the chemical reintercalation of lithium ions in the $Li_{2/3}MO_2$ structures leading to structures such as $Li_{(2/3+x)}[Ni_{1/3}Mn_{2/3}]O_2$ and $Li_{(2/3+x)}[Co_{0.15}Mn_{0.85}]O_2$ [7,8]. To better understand the exchange reaction mechanism we attempt to study the exchange reaction of the P2−$Na_{0.70}CoO_2$ phase.

In the companion paper (Part I), we have proposed a structural model for the P2→O2 transition [9]. The driving force of this transition is the formation of octahedral environments for lithium ions which are obtained when one slab over two glides by (2/3, 1/3, 0) or by (1/3, 2/3, 0) in the P2 structure. The exchange reaction consists on the formation of O2-type nucleation centers and then on their growth into the P2 crystals. The existence of two different gliding vectors should lead to stacking faulted structures that can be simulated using the DIFFaX software. Three series of simulation of stacking faulted structures have been achieved,

*Corresponding author. Fax: +33-540006698.
E-mail address: crog@icmcb.u-bordeaux1.fr (L. Croguennec).

0022-4596/$ - see front matter © 2004 Elsevier Inc. All rights reserved.
doi:10.1016/j.jssc.2004.04.028

considering previous hypotheses for the nucleation: the first one was a simplified case to explain the nucleation—growing phenomenon with only one type of slabs concerned by the nucleation, the second one was the general case (two types of slabs as possible nucleation centers and two possible gliding vectors (2/3, 1/3, 0) or (1/3, 2/3, 0)) and the third one was the general case with possibilities of sodium remaining in the final structure and, therefore, of prismatic (P)-type defects. This study has shown that depending on the ratio between the growing and nucleation speeds, O2, O6 or faulted structures are obtained and that this model allows a good analysis of the exchange process. The comparison of simulated and experimental XRD patterns for O2–$LiCoO_2$ has finally shown that in that specific case the growth of O2 domains in P2 crystals is faster than the formation of nucleation centers, leading thus to a closely ideal O2 phase with large O2 blocks and defects at the boundaries between these blocks.

We will now present the in situ X-ray diffraction study of the exchange reaction of sodium by lithium in P2$-Na_{0.7}CoO_2$ and, especially, the mechanisms proposed to explain the P2$\rightarrow$O2 transition. We will then check if the model proposed for the nucleation in the companion paper (Part I) from the study of the final material is in good agreement with the whole reaction process.

2. Experimental

2.1. X-ray diffraction

The XRD patterns recorded in situ during the ion exchange of sodium by lithium in P2$-Na_{0.70}CoO_2$ were obtained using an INEL CPS 120 curve position sensitive detector with Co$K\alpha$ radiation. Note that in order to facilitate the comparison with XRD data obtained on other diffractometers, all these XRD patterns will be reported using the Cu$K\alpha$ radiation as reference. A home-made sample-holder, represented in Fig. 1 and previously developed for in situ XRD studies of alkaline batteries upon cycling, was used to perform this exchange in situ. Its cavity below the reference plane was used as a tank for the salt solution and its Kapton® window allowed to record XRD patterns without any contact with the air and, therefore, to prevent any carbonatation of the salt solution during the experiment. A mixture of 100 mg of P2$-Na_{0.70}CoO_2$ and 10 mg of Ni powder (used as reference to correct for the sample displacement) was pressed (1 ton during 5 min) on a $30 \times 5\,mm^2$ nickel foam in an argon-filled dry box. This sample was then placed in the XRD sample-holder, in the reference plane, in contact with a 5 M aqueous solution (Li/Na $\approx$ 5) of LiCl|LiOH (1:1). A total of 64 XRD patterns was recorded during 16 h, with 10 min acquisition time for each XRD pattern and 5 min waiting time between two data recording. Note that the use of a curve detector to perform this experiment allowed to get XRD patterns with a good resolution, in short acquisition times. The accurate determination of the peak positions was done using the PROFILE peak-search program [10], assuming a pseudo-voigt line shape. The size of the crystallites (assumed to be equal to the coherence length) was estimated using the Scherrer formula. In order to determine the apparatus contribution to the line broadening, the very well crystallized $Na_2Ca_3Al_2F_{14}$ compound was used as reference.

The simulation of XRD patterns was done using the DIFFaX program [11], all the explanations were given in the companion paper (Part I) [9].

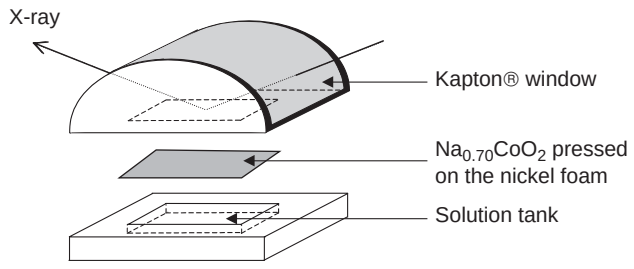

Fig. 1. In situ cell for the XRD study of the exchange reaction.

2.2. Electrochemistry

Electrochemical measurements were carried out at room temperature (25°C) for the Li//Li_xCoO_2, Na//Na_xCoO_2 and Li//Na_xCoO_2 cells. The positive electrodes consisted of a mixture of 88% by weight of active material, 2% of PTFE (polytetrafluorethylene) and 10% of a mixture (1:1) of graphite and carbon black. The electrolyte used for the lithium batteries was 1 M $LiPF_6$ dissolved in a mixture of propylene carbonate (PC), ethylene carbonate (EC) and dimethyl carbonate (DMC) (1:1:3 by volume). The electrolyte used for the sodium batteries was 1 M $NaClO_4$ dissolved in PC. The cells, assembled in an argon-filled dry box, were cycled at 400 $\mu A\,cm^{-2}$ (active mass = 15 mg, $C/20$ rate).

3. Results

3.1. General description

Fig. 2 shows the XRD patterns obtained during the exchange reaction: it clearly appears that two different steps occur during the reaction. In the first step, during the first 4 h, the amount of O2 phase is almost negligible, then at the beginning of the second step it increases

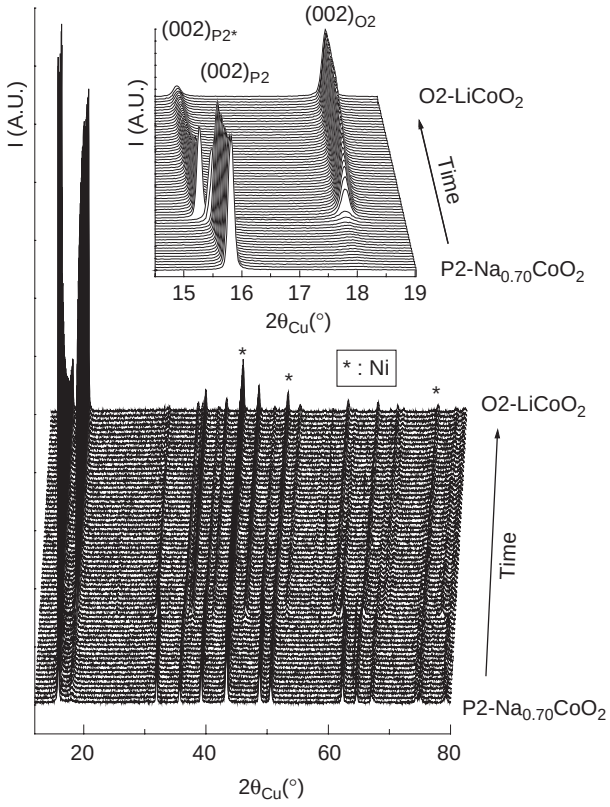

Fig. 2. XRD patterns recorded in situ during the exchange of sodium by lithium in P2−$Na_{0.70}CoO_2$. A total of 64 XRD patterns was recorded during 16 h, with 10 min acquisition time for each pattern and 5 min waiting time between two patterns.

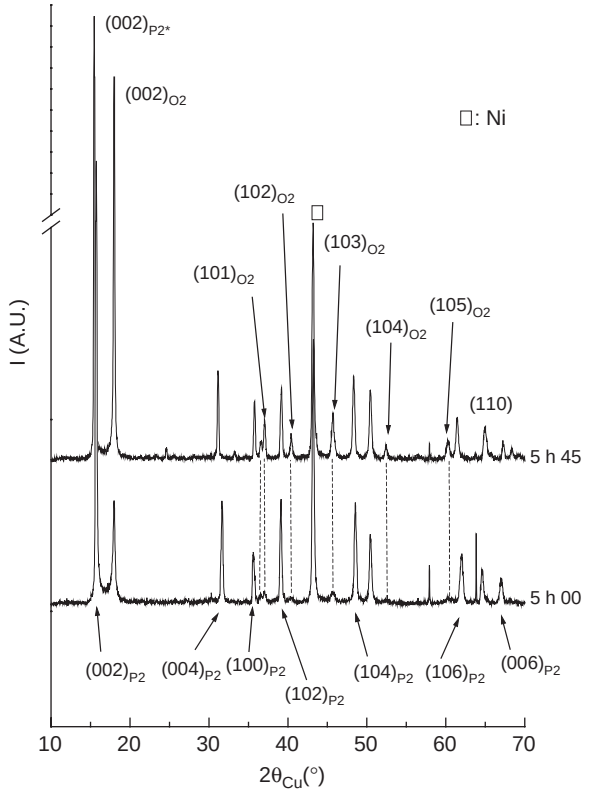

Fig. 3. Comparison of the XRD patterns recorded just before and just after the P2→P2* phase transition.

suddenly and simultaneously the interslab distance of the remaining P2 phase increases. This effect is evidenced on the enlargement of the XRD patterns (14.5–19°/$2\theta_{Cu}$ range). In the following we will name P2* the new sodium phase formed during the exchange process. Note that on the experimental in situ XRD patterns, and on the contrary to what is observed on the ex situ XRD pattern, all the (00*l*) lines are more intense than expected due to the important preferential orientation caused by the sample preparation (powder pressed on the nickel foam). The XRD patterns recorded just before and just after the P2→P2* phase transition are presented in Fig. 3; after 5 h all the diffraction lines of the O2 phase are present, but with a very small intensity. The P2* phase can be indexed as P2−$Na_{0.70}CoO_2$ in the $P6_3/mmc$ space group with $a_{hex.}$ and $c_{hex.}$ cell parameters, respectively, smaller and larger than those observed for the starting P2−$Na_{0.70}CoO_2$ phase (Table 1). This evolution suggests that there is an oxidation of P2−$Na_{0.70}CoO_2$. Indeed, the removal of sodium ions from the structure induces increasing electrostatic repulsions between adjacent oxygen layers through the interslab space and thus an increase of $c_{hex.}$. Furthermore, the oxidation of the cobalt ions induces a decrease of the metal–metal distance and, therefore, of $a_{hex.}$. By

Table 1
Cell parameters of P2–$Na_{0.70}CoO_2$ and P2*–$Na_{\sim 0.50}CoO_2$ phases

Cell parameters (Å)	P2–$Na_{0.7}CoO_2$	P2*–$Na_{\sim 0.5}CoO_2$
$a_{hex.}$	2.833(4)	2.808(3)
$c_{hex.}$	10.81(1)	11.02(1)

comparison with the results obtained electrochemically by Braconnier et al. for the Na//P2−Na_xCoO_2 system, it can be assumed that P2* corresponds to $Na_{\sim 0.5}CoO_2$ [12]. Note that the residual P2 phase observed by Carlier et al. after ex situ exchange reactions in water, hexanol and methanol, corresponds also to the P2* phase (see Fig. 3 in Ref. [13]). At the end of the in situ experiment, the P2* phase remains in a larger amount than at the end of the exchange made ex situ, suggesting that the reaction was not totally achieved. This behavior can result from the smaller excess of LiCl|LiOH used in the in situ experiment versus the classical exchange one.

The evolution of the FWHM of (002) diffraction lines, of the various phases versus the reaction time is given in Fig. 4. Note that those FWHMs give directly the coherence length perpendicularly to the slabs. Fig. 5 shows thus the evolution of the average size of the O2 domains (given in number of slabs) during the exchange reaction. The slope of the line represented in each

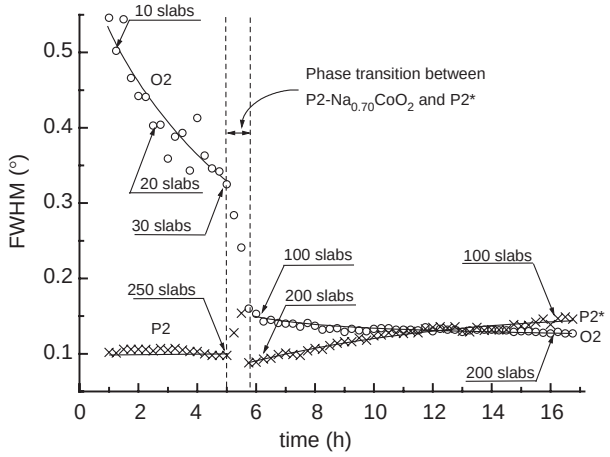

Fig. 4. Evolution of the FWHM of the (002) diffraction lines for the $P2-Na_{0.70}CoO_2$, $P2^*-Na_{\sim 0.50}CoO_2$ and $O2-LiCoO_2$ phases, during the ion-exchange reaction. The coherence lengths, calculated from experimental FWHMs using the Scherrer formula, are also given.

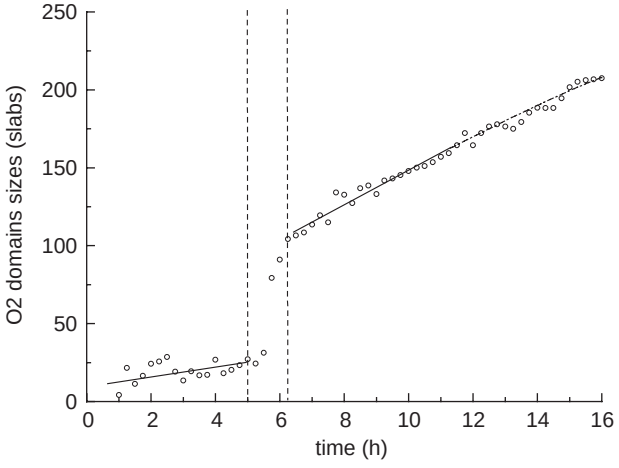

Fig. 5. Evolution of the average size of the O2 domains (in number of slabs) during the exchange reaction.

domain (before and after the $P2 \rightarrow P2^*$ phase transition) is related to the growth rate of the O2 domains. At the beginning of the exchange reaction, the FWHM of the $(002)_{P2}$ diffraction line remains almost constant, the coherence length is equal to 1400 Å which corresponds to about 250 slabs. This value must be compared to the coherence length of the starting P2 phase before the exchange. In this case, the Scherrer formula gives a coherence length of 4400 Å (around 800 slabs) in good agreement with the Scanning Electron Microscopy study, which shows that the average thickness of $Na_{0.7}CoO_2$ crystallites without apparent defects is close to 5000 Å (corresponding to 900 slabs). The accuracy of this coherence length value is very small because the involved FWHM value is close to the limit one to use the Scherrer formula. Nevertheless, the comparison of the values before and after exchange shows that the P2 domain thickness decreases very quickly at the very beginning of the exchange reaction, then it remains almost constant during the following 4 h. The first XRD pattern has been recorded 1 h after the beginning of the exchange reaction. This hour corresponds to the time required to assemble the cell and to start the experiment after the exchange solution introduction. On the first XRD pattern, the (002) diffraction line of the O2 phase appears clearly. It is very broad and it corresponds to 10 slabs. Then, this (002) diffraction line narrows continuously in an almost linear process. After 5 h, it corresponds to O2 domains with 30 slabs. All these results give only a tendency, because it is well known that the Scherrer formula is a very crude model. The $P2 \rightarrow P2^*$ phase transition occurs just after 5 h of reaction time and is associated to a sudden increase, immediately followed by a decrease, of the FWHM of the $(002)_{P2}$ line. This behavior suggests the formation of an intermediate P2 phase with a distribution of distances along the *c*-axis. At this transition, the FWHM of the $(002)_{O2}$ peak decreases suddenly and then decrease slowly until the end of the exchange reaction. As shown by the strong increase of the line intensity, a significant part of the $O2-LiCoO_2$ phase is thus formed after 5 h, only the proportion of the O2 and $P2^*$ phases changes afterwards. As shown in Fig. 5 by the comparison of the slopes of the two lines, after the $P2 \rightarrow P2^*$ phase transition the growth rate is highly increased (i.e. four times higher than the initial one). It should be noted that after the formation of the $O2-LiCoO_2$ phase, the FWHM of the $(002)^*_{P2}$ line increases continuously. As explained just before, this evolution is certainly related to the size of the residual small $P2^*$ domains in $O2-LiCoO_2$ crystals.

During this ion exchange reaction, only slab glidings are at the origin of the $P2-Na_{0.70}CoO_2 \rightarrow O2-LiCoO_2$ phase transition. Therefore, in such a case, a P2–O2 intergrowth with a continuous change in the ratio between the two phases could explain the evolution of the FWHMs. Note that the overall number of slabs remains almost constant ($\sim$300 slabs) after the initial nucleation of the reaction.

3.2. Simulation of P2–O2 intergrowths during reaction

In order to determine if small domains of O2 in $P2-Na_{0.70}CoO_2$ crystals are large enough for the coherence length to induce diffraction and thus observation of the $(002)_{O2}$ diffraction line, XRD patterns associated to P2–O2 intergrowths were simulated using the DIFFaX software. In the companion paper (Part I), we have shown that the small amount of defects found in the O2 final phase resulted from a high growth speed versus the nucleation one. Therefore, the simulations of P2–O2 intergrowths were done assuming the existence of ideal O2 domains within the P2 structure. Starting from

a P2 crystal with about 250 slabs, the number of slabs involved in the O2 structure was gradually increased. In the previous paper, we have reported in detail the way to describe a given packing to simulate its XRD pattern using the DiFFaX software. Fig. 6 presents thus the ideal P2 phase packing and an example of P2–O2 intergrowth, with the associated stacking vectors (R_{ij}) and probabilities (α_{ij}). To built up the P2–O2 intergrowth using DIFFaX, three AB-type slabs and three BA-type slabs were used: one of each for the P2 description (slabs **(1)** and **(2)**) and the others for the two O2 descriptions (growth from a BA-type slab (slabs **(3)** and **(4)**) and from AB-type slab (slabs **(5)** and **(6)**)). In order to take into account the difference in interslab distances between P2 and O2, the stacking vectors are (α, β, $c_{\mathrm{hex.(P2)}}/2$) and (α', β', $c_{\mathrm{hex.(O_2)}}/2$) in P2 and O2 domains, respectively. As shown in Fig. 6, the probability associated to the **(1)→(6)** and the **(2)→(3)** transitions fixes the average size of the P2 and O2 domains, because these transitions initiate the growth of an O2 domain in the P2 crystals. With a probability of 0.4% (1/250), there is one chance every 250 P2-type slabs to begin the formation of a new O2 domain, in good agreement with an average size of 250 slabs for the P2 domains (Fig. 4). For the O2 domains, one over the two transitions is associated to a probability equal to one (**(6)→(5)** or **(3)→(4)**) and the other (**(5)→(6)** or **(4)→(3)**) to a probability equal to $(1-1/(n/2))$, with n the average number of slabs in O2 domains. The end of the O2 domain is reached when the **(5)→(2)** or **(4)→(1)** transition occurs with a probability equal to $1/(n/2)$. The atomic positions within the AB- and BA-type slabs are given in Table 2, whereas the probabilities of transition and the stacking vectors associated are given in Table 3. Fig. 7 shows the XRD patterns calculated for

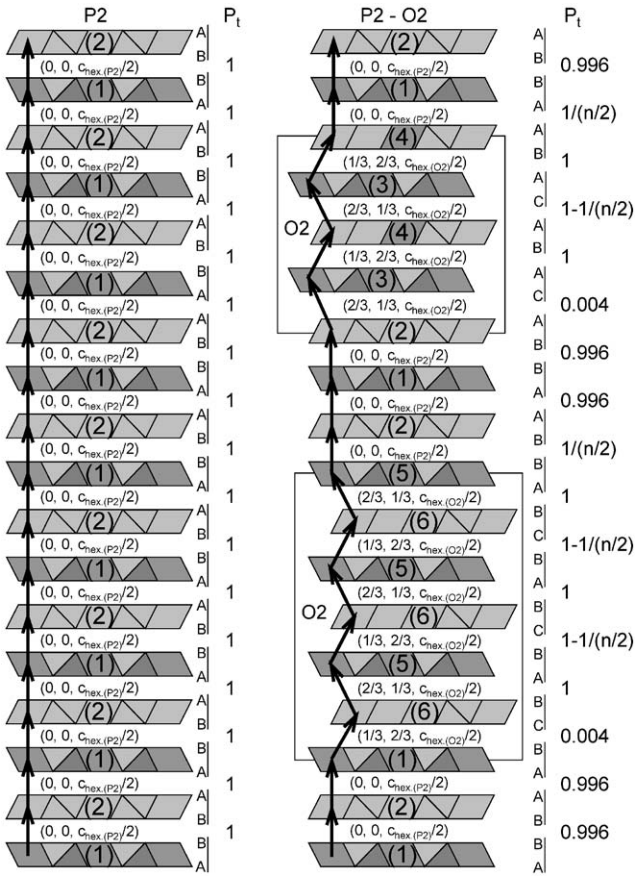

Fig. 6. Scheme of the structural models used by DIFFaX software in order to simulate the XRD pattern for pure P2 phase (a) and for P2–O2 intergrowth (b). The stacking vectors and the associated probabilities are also given.

Table 3
Structural model used for the calculation of the XRD patterns for P2–O2 intergrowths

$(i)\rightarrow(j)$	α_{ij}	R_{ij}		
		R_{xij}	R_{yij}	R_{zij}
(1)→(2)	0.996	0.0000	0.0000	0.5719
(1)→(6)	0.004	1/3	2/3	0.5000
(2)→(1)	0.996	0.0000	0.0000	0.5719
(2)→(3)	0.004	2/3	1/3	0.5000
(3)→(4)	1	1/3	2/3	0.5000
(4)→(1)	$1/(n/2)$	0.0000	0.0000	0.5719
(4)→(3)	$1-(1/(n/2))$	2/3	1/3	0.5000
(5)→(2)	$1/(n/2)$	0.0000	0.0000	0.5719
(5)→(6)	$1-(1/(n/2))$	1/3	2/3	0.5000
(6)→(5)	1	2/3	1/3	0.5000

Translation probabilities (α_{ij}) and translation vectors (R_{ij}: R_{xij}, R_{yij}, R_{zij}) associated to the stacking of the slabs no. j above the slabs no. i. The probability of creating O2 domains is 0.4% (which gives an average size of 250 slabs for the P2 domains). The n variable represents the average number of slabs necessary to describe the O2 domains.

Table 2
Description of the AB-type slabs (slab no. 1, slab no. 3, …, slab no. 5) and of the BA-type slabs (slab no. 2, slab no. 4, …, slab no. 6)

	Slab no. **(1)**, **(3)**, **(5)**				Slab no. **(2)**, **(4)**, **(6)**			
	AB-type				BA-type			
	x	y	z	Occ.	x	y	z	Occ.
Co	0.0000	0.0000	0.0000	1.00	0.0000	0.0000	0.0000	1.00
O(1)	2/3	1/3	−0.1100	1.00	2/3	1/3	0.1100	1.00
O(2)	1/3	2/3	0.1100	1.00	1/3	2/3	−0.1100	1.00

The cell parameters used are $a_{\mathrm{hex.}} = b_{\mathrm{hex.}} = 2.8035$ Å and $c_{\mathrm{hex.}} = 9.540$ Å.

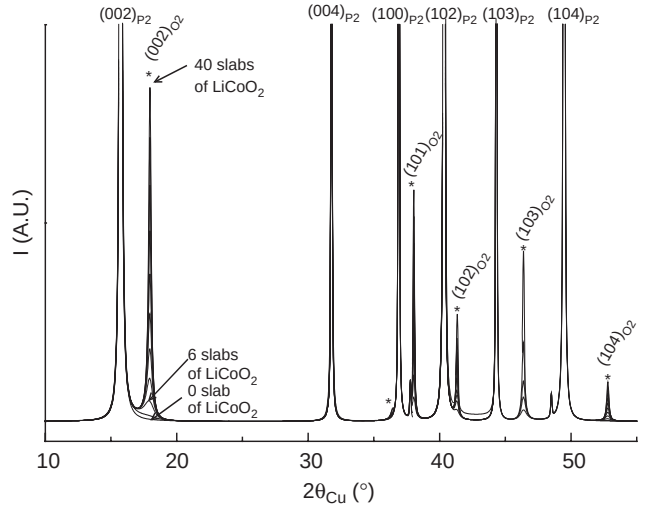

Fig. 7. XRD patterns calculated for P2–O2 intergrowths. * indicates the O2–$LiCoO_2$ peak positions. The average size of the O2 domains varies from 0 to 40 slabs.

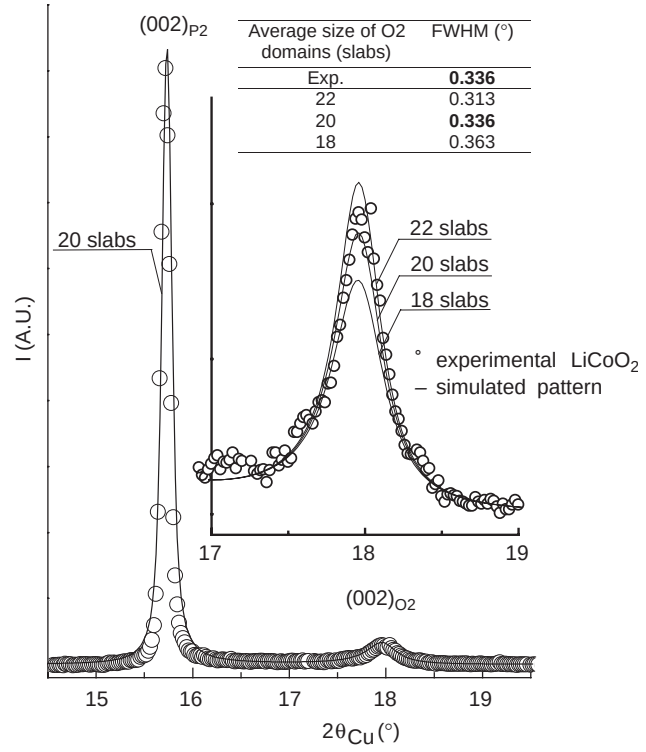

Fig. 8. Comparison between the experimental XRD pattern recorded just before the P2→P2* phase transition and the pattern calculated for an average size of 20 slabs for the O2 domains in the P2−$Na_{0.70}CoO_2$ crystals. Enlargement of the $(002)_{O2}$ diffraction line with the patterns calculated for an average size of 18, 20 and 22 slabs for the O2 domains and the corresponding FWHMs is also reported.

P2–O2 intergrowths with an average size of 250 slabs for P2 and an increasing number of O2 slabs (between 0 and 40). The diffraction lines associated to O2–$LiCoO_2$ (noted with "*") clearly appear when the average size of the O2 domains becomes larger than six successive slabs within an initial P2 crystal.

The comparison of the experimental and simulated XRD patterns has then been achieved, especially by taking into account the first (00*l*) diffraction line of each phase, that allows to determine the number of slabs involved. Fig. 8 shows in the [14°–20°] ($2\theta_{Cu}$) range comparison between the experimental pattern recorded after 4 h of reaction time and the patterns calculated for P2–O2 intergrowth with O2 domains with an average size of 18, 20 and 22 consecutive slabs. The best agreement is obtained with an average size of 20 consecutive slabs, in rather good agreement with the coherence length calculated from the experimental FWHM for the O2 domains using the Scherrer formula. Indeed, the experimental FWHM of the $(002)_{O2}$ diffraction line, despite a small accuracy due to low intensity, leads to 150 Å domains, i.e. to 30 slabs (Fig. 4).

4. Discussion

Starting from a P2−$Na_{0.70}CoO_2$ crystal with an average size corresponding to 800 slabs, it appears that after 1 h of exchange reaction, there are only a few nucleation centers (one every 250 slabs in average). Then during the first step of the exchange process (5 h), there is only a slow growing of the O2 domain without other nucleation (in first approximation). As we have discussed in the conclusion of the companion paper (Part I), the difference in Co–Co interslab distances between the O2−$LiCoO_2$ and P2−$Na_{0.70}CoO_2$ domains leads to a destabilization of the interslab spaces adjacent to the O2−$LiCoO_2$ domains. Therefore, the growing of an O2 domain is easier in that case than the nucleation of a new one.

After 5 h of reaction time, the size of the O2 domains is still small (30 slabs), but within 1 h, associated to the P2→P2* phase transition, it raises quickly to 100 slabs whereas the size of the P2* domains decreases to 200 slabs. Then during the following 10 h the exchange continues but more slowly. Since the process involved when the P2* phase appears is obviously related to redox reactions, we have compared the electrochemical behavior of P2–Na_xCoO_2 and O2–Li_xCoO_2 in sodium and lithium batteries, respectively. Fig. 9 shows the electrochemical curves, voltage$=f(x)$, obtained for Li//Li_xCoO_2 and Na//Na_xCoO_2 cells. Note that an Li/$NaClO_4$/Na_xCoO_2 cell was made in order to compare the potential of the Na_xCoO_2 phase in a sodium cell and in a lithium cell. It appears that there is an 0.3 V difference in potential due to the difference in negative electrode materials. As illustrated schematically in Fig. 9, the formation of O2−Li_xCoO_2 domains in

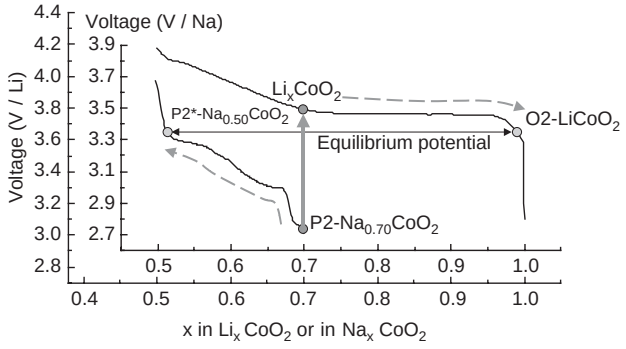

Fig. 9. The voltage $=f(x)$ electrochemical curves obtained for the $Li//Li_xCoO_2$ and $Na//Na_xCoO_2$ systems. Note that for a given phase, an 0.3 V difference in potential is observed between a sodium and a lithium cell.

$P2-Na_{0.70}CoO_2$ crystals induces, therefore, locally a high 3.8 V potential versus Li. In order to balance the potential all over the crystal, there are probably simultaneously the oxidation of $P2-Na_{0.70}CoO_2$ to $P2^*-Na_{\sim 0.50}CoO_2$ and the reduction of $O2-Li_xCoO_2$ to $O2-Li_{x\approx 1}CoO_2$. The further reduction of Li_xCoO_2 occurs through the oxidation of water (from the salts solution) as shown by the equation: $2Co^{4+}+H_2O \rightarrow 2Co^{3+}+2H^+ + \frac{1}{2}O_2$. Note that a gas release was observed during the in situ experiment through the formation of bubbles.

After the $P2 \rightarrow P2^*$ transition, two factors have to be taken into account in order to discuss the exchange mechanism:

- The Co–Co distances in the P2 oxidized $P2^*$ phase are now very close to the O2–$LiCoO_2$ ones (2.808 and 2.804 Å, respectively), therefore the driving force due to the distance mismatch is no more involved. This thus leads to a more difficult growth of the O2 domains.
- The decreasing of sodium in the $P2^*$ structure induces an enlargement of the P2 interslab space which leads to an increase of the lithium diffusion through the structure and therefore which should induce a large increase of the kinetic of the exchange reaction.

As shown by the increase of the rate of the exchange reaction after the $P2 \rightarrow P2^*$ transition, the increase of the lithium diffusion in the crystallites plays the most important role.

Acknowledgments

The authors wish to thank CNES and Région Aquitaine for financial support.

References

[1] C. Delmas, J.J. Braconnier, P. Hagenmuller, Mater. Res. Bull. 17 (1982) 117.
[2] J.M. Paulsen, C.L. Thomas, J.R. Dahn, J. Electrochem. Soc. 147 (2000) 2862–2867.
[3] Z.H. Lu, R.A. Donaberger, C.L. Thomas, J.R. Dahn, J. Electrochem. Soc. 149 (2002) A1083–A1091.
[4] J.M. Paulsen, C.L. Thomas, J.R. Dahn, J. Electrochem. Soc. 146 (1999) 3560.
[5] J.M. Paulsen, R.A. Donaberger, J.R. Dahn, Chem. Mater. 12 (2000) 2257–2267.
[6] Z.H. Lu, J.R. Dahn, Chem. Mater. 13 (2001) 2078.
[7] K.M. Shaju, G.V.S. Rao, B.V.R. Chowdari, Electrochem. Commun. 4 (2002) 633–638.
[8] K.M. Shaju, G.V. Subba Rao, B.V.R. Chowdari, Solid State Ionics 152–153 (2002) 69–81.
[9] F. Tournadre, L. Croguennec, I. Saadoune, D. Carlier, Y. Shao-Horn, P. Willmann, C. Delmas, J. Solid State Chem., accepted for publication.
[10] Diffrac-At, Siemens and Socabim, 1993.
[11] R.D. Shannon, C.T. Prewitt, Acta Crystallogr. B 25 (1969) 925.
[12] J.J. Braconnier, C. Delmas, C. Fouassier, P. Hagenmuller, Mater. Res. Bull. 15 (1980) 1797.
[13] D. Carlier, I. Saadoune, E. Suard, L. Croguennec, M. Ménétrier, C. Delmas, Solid State Ionics 144 (2001) 263–276.